The feasibility of vitrifying a sandstone enclosure in the British Iron Age

Fabian B. Wadsworth[1], David E. Damby[1], Rebecca L. Hearne[2,3], Jennifer S. Le Blond[4,5], Jérémie Vasseur[1], Jens Najorka[5], Kai-Uwe Hess[1], Donald B. Dingwell[1]

1 Earth and Environmental Sciences, Ludwig-Maximilians-Universität, Theresienstr. 41, 80333 Munich, Germany.
2 University of Leicester Archaeological Services, School of Archaeology and Ancient History, University of Leicester, University Road, Leicester, LE1 7RH, UK.
3 Department of Archaeology, University of Sheffield, Northgate House, West Street, Sheffield, S1 4ET, UK.
4 Department of Earth Sciences and Engineering, Imperial College London, London, SW7 2AZ, UK.
5 Department of Mineralogy, Natural History Museum, Cromwell Road, London, SW7 5BD, UK.

Keywords: vitrified forts; glass; quartz transition; cristobalite; Wincobank

Iron Age structures with evidence for having been subjected to high temperatures have been identified throughout Europe. The thermal conditions that must have yielded such evidence of alteration remain enigmatic, especially for the case of high-silica, quartz-rich building materials such as sandstones. Here, we conduct an experimental investigation of thermal treatment using the Wincobank Iron Age hill fort site in Sheffield, South Yorkshire (U.K.) as a test case. We have selected samples of the unaltered protolithic sandstone from which the fort was constructed as starting material as well as material from the vitrified wall core. An experimental suite of thermally treated protolith samples has been analysed using a combined approach involving X-ray diffraction and thermal analysis (simultaneous differential scanning calorimetry with thermogravimetric analysis). Comparison between our experimental products and the variably vitrified samples found in the wall of the Wincobank hill fort help to constrain firing temperatures and timescales. For mineralogical markers, we employ the high-temperature conversion of quartz to cristobalite and the melting of feldspar to compare the relative abundance of these phases before and after thermal treatment. We find that the Iron Age wall samples have mineralogical abundances most consistent with a minimum firing temperature range <1100-1250 °C and a firing timescale of >10 hours. These first quantitative constraints for a fort constructed of sandstone are consistent with those found for forts constructed of granitic material. Finally, we explore the reasons for thermal disequilibrium during firing and invoke this mechanism to explain the differential vitrification found at some Iron Age stone-built enclosures.

1. Introduction

Vitrified forts are anthropogenic archaeological stone-built structures which contain a glass, or devitrified product of a glass, as a phase in the stonework which is surmised to have been produced through *in situ* exposure to high temperatures. Such forts have been identified throughout Europe (e.g. Youngblood, et al., 1978, Kresten, 2004) and are abundant in Scotland (MacKie, 1969, MacKie, 1976, Nisbet, 1974, Friend, et al., 2008). Despite a large sample of sites, ambiguity remains concerning the vitrification mechanism, temperatures, kinetics and motives (e.g. Mackie, 1976).

Opinion appears to have converged on a consensus that vitrification is largely an intentional rather than accidental consequence of high temperature treatment of the stonework enclosing the forts (e.g. Youngblood, et al., 1978, Nisbet, 1974, Brothwell, et al., 1974). The specific prehistoric intentions for vitrification however are not constrained. Hearne (2015) summarises the arguments for intentional vitrification motives in 3 categories: (1) strengthening of the walls (Nisbet, 1974, Brothwell, et al., 1974); (2) intentional destructive attack (Cotton, 1954, Small and Cottam, 1972); or (3) a hitherto poorly understood ritual or cultural practice (Bowden and McOmish, 1987). Experimental work constraining the conditions required for vitrification may provide useful insights for deciding the relative likelihood of these three potential mechanisms (e.g. Youngblood et al., 1978). The enigmatic nature of these Iron Age vitrified structures makes them a topic ripe for ongoing study.

The temperatures required for vitrification have been constrained for granitic (*sensu lato*) building materials to a range with a lower boundary defined by the solidus (~925 °C for dry granites; Youngblood et al., 1978). As there is no direct evidence that complete melting is ubiquitously achieved in any vitrified fort, the upper boundary is likely to be below the liquidus (i.e. <1250 °C for dry granites; Youngblood et al., 1978). Often defined is an upper temperature at which the authors propose that the melt fraction - preserved as glass containing quench crystals produced upon cooling - was in equilibrium with the crystal assemblage (Youngblood, et al., 1978, Friend, et al., 2007). If the solidus and liquidus are to represent absolute bounds for the vitrification process and if no material-independent general temperature range applies, then the very quartz-rich systems of sandstone-made forts remain substantially less well-constrained than is the case for "granitic" forts.

Firing of experimentally constructed walls has yielded large-scale confirmation that vitrification is possible in a reconstructed setting using the timber-frame construction thought to be prevalent in the Iron Age (Childe and Thorneycroft, 1938, Ralston, 1986). Similarly, sample-scale experimental work has provided additional constraints on the temperature and timescales required for vitrification (Hearne, 2015; Friend et al., 2008; Friend et al., 2007) although these latter experiments have never been scaled to the conditions likely exhibited in large experimental firings.

Here we use the sandstone building material used in the construction of the Wincobank hill fort site (Sheffield, South Yorkshire, U.K.; Hearne, 2015) to provide a sample-scale experimental suite covering a large temperature (600-1400 °C) and time (0-20 hours) window. We compare the thermal and mineralogical results with those from a suite of variably vitrified wall samples

80 at the same fort in order to constrain the range of conditions required to produce the Iron Age
81 examples. Finally, we illustrate an example of the importance of scale when considering the
82 distribution of heat, and therefore vitrification potential, in a sandstone wall. In all of this we
83 build on the work by Hearne (2015) who was the first to employ this experimental approach
84 with Wincobank hill site material.

85

2. Materials and methods

2.1 Sample selection

Samples were exclusively collected from Wincobank hill fort site (dated to BCE 530-470; Beswick, 1987; Beswick, 1985), which is built from the locally-sourced sandstone (hereafter referred to as the protolith). Samples were selected to represent (1) material that had undergone no thermal alteration and thus can be considered to be the raw protolith material from which the Wincobank enclosure(s) were formed and (2) material from the thermally altered parts of the walls (hereafter referred to as the vitrified samples). The protolith material is ubiquitous in the earthwork construction and outcrops locally as blocks of massive orange sandstone which exhibits minor laminations or small-scale bedding as their only distinguishing textural feature. The vitrified samples found in the site wall differ from the protolith to a variable extent via textural features including red discolouration, black discolouration with a glassy lustre, local vesiculation and fluidal textures (Fig. 1; Hearne, 2015). The specific sampling locations were from various locations on the south side of the enclosure but the poor surface exposure precluded systematic sampling from external to internal edge of the wall itself and we did not undertake excavation. The vitrified samples *Wall 1-4* are chosen to represent the qualitative range of vitrification seen at the site.

2.2 X-ray powder diffraction (XRD)

In order to discern whether the difference in phases resulting from thermal treatment mimicked that observed between protolith and vitrified samples, the mineralogy of the protolith, the vitrified material and the experimental samples was determined by powder X-ray diffraction (XRD) at the Natural History Museum in London. Samples were ground in an agate mortar and ~30 mg loaded into 6.9 mm diameter, 1 mm depth circular well mounts. XRD data were collected using an Enraf-Nonius PDS120 diffractometer with an INEL 120° curved position sensitive detector (PSD). We used a combination of primary monochromator (Ge 111) and slit system to select only Cu $K\alpha_1$ radiation and define the incident beam size. Tube operating conditions were 40 kV and 35 mA. The angle between the incident beam and the sample surface was maintained at 4.0° with the sample spinning to improve count statistics. For the detailed investigation of phyllosilicates, an aliquot of each sample was prepared as an oriented mount on a glass slide. This technique encourages preferred orientation of clay particles parallel to the glass slide surface and enhances the intensity of basal reflections [001]. A suspension of soil was prepared, sonicated for 1 minute and 0.5 ml pipetted onto a clean glass slide and left to dry in air. For this part of the analysis we used a PANalytical X'Pert-PRO diffractometer (240 mm radius) with a step size of 0.02° 2θ, a total count time of 90 minutes over a scan range of 2-80° 2θ. The PDF-2 database from ICDD (International Centre for Diffraction Data, http://www.icdd.com) was used to perform the phase identification in the diffraction patterns.

The relative proportions of quartz and cristobalite were evaluated using the areal intensities of their highest intensity peaks. A linear baseline was subtracted from the peak associated with

quartz at 26.6° 2θ and the peak associated with cristobalite at 21.8° 2θ. The overlap of a minor feldspar peak with the primary cristobalite peak at ~22.0° 2θ was ignored for relative phase quantification since feldspar tended to melt prior to cristobalite crystallisation in our experimental samples (e.g. see Fig. 5) and no wall sample contained both phases.

2.3 Thermal analysis

Differential scanning calorimetry (DSC) and thermogravimetry (TG) measurements were made using a Netzsch® 404 C Pegasus and a Netzsch® 449 C Jupiter, respectively. Samples of protolith and vitrified samples from the Wincobank site were powdered to a particle size distribution with a dominant fraction at 90-125 µm but not further sieved to avoid segregation of phases. 30-40 mg of each were loaded into platinum crucibles with lids. A static air atmosphere was used in all experiments as tests have revealed that the effect of using a more reducing argon atmosphere on the results was negligible within analytical error.

Protolith samples were exposed to two DSC heating cycles. The first cycle was designed to expose the sample to a particular temperature (600-1400 °C peak temperature) for a pre-determined duration (0, 10 or 20 hours); the second cycle was to assess the thermal properties imparted to the sample during the first cycle. During both the first and second heating cycles, samples were initially allowed to thermally equilibrate at 100 °C for 20 minutes. During the first cycle, all samples were heated to the experimental temperature at 25 °C.min^{-1} and held for a dwell time of 0-20 hours before cooling at 25 °C.min^{-1} to ambient temperature. During the second heating cycle samples were heated to 1400 °C at 25 °C.min^{-1}. A sampling rate of 40 Hz was used to ensure high resolution. The S-type thermocouples in both the DSC and TG instruments were calibrated to ±1.5 °C. Baseline measurements were made on the same empty crucibles under the same experimental conditions and were subtracted from the sample curves.

Endothermic heat flow peaks interpreted to represent the α-β quartz transition (575-577 °C) were integrated between 550 and 600 °C using a linear regression as a baseline. The integrated value from the second heating cycle is calculated relative to that from the first cycle. Thermally altered samples from the Wincobank site were also measured in this way and their integrated peaks are obtained relative to an average value for the protolith on the first heating cycle (i.e. the unaltered transition). The area under the peak associated with the α-β transition in quartz is proportional to the amount of quartz, such that relative changes prior to and following high temperature alteration are quantitative. The absolute peak position of the α-β transition in quartz is weakly dependent on the heating rate. By always using heating and cooling rates of 25 K.min^{-1} in this study, the relative changes in peak area are always comparable. This means that the peak temperatures for this transition quoted here (Supplementary Fig. 1), are not to be compared with other studies where different heating rates were applied. No heating rate correction was performed.

2.4 Bulk composition by X-ray fluorescence (XRF)

The protolith and sample *Wall 4* were milled to <63 µm particle size in acetone, dried, ignited and mixed with spectromelt A12 (66 % di-lithium tetraborate, 34 % lithium metaborate) flux at a sample to flux ratio of 1:9. Mixtures were prepared as fused glass tablets prior to analysis. The XRF measurements were obtained using a Philips MagiX Pro WDX-XRFS at LMU, Munich.

Results

2.5 The protolith

The protolith is a brown-orange fine-grained sandstone composed dominantly of quartz with minor components of feldspar and kaolinite and muscovite (Fig. 2). Additional trace components not resolved by XRD in this study (<<1 wt %) may include rutile, chrome spinel and zircon (Hallsworth and Chisholm, 2000). On heating, the protolith shows an endothermic peak in heat flow at ~576 °C diagnostic of the *α-β* transition in quartz, consistent with the dominantly quartz mineralogy. Note that the absolute position of the transition is heating-rate dependent (Section 2.3). The bulk chemistry is quoted in Table 1.

2.6 Samples from the wall at the Wincobank hill site

Variably altered and vitrified samples from the Wincobank hill site are texturally distinct from the protolith. They exhibit (1) red discolouration, (2) black and glassy lustre or (3) textural overprinting by local vesicularity in the areas of prodigious glassy texture. The mineralogy of the vitrified samples consists of quartz and either feldspar or cristobalite with possible? trace amounts of sekaninaite. Sample *Wall 1* contains only quartz and feldspar, similar to the protolith, and is discoloured to a deep orange, while samples *Wall 2*, *Wall 3* and *Wall 4* are discoloured to dark brown or black with glassy lustre and contain only quartz and cristobalite, unlike the protolith (Fig. 3). The 3 samples that contain cristobalite also show a noisy endothermic peak in heat flow at ~269 °C consistent with the *α-β* transition of cristobalite, followed by a second endothermic heat-flow peak at ~576 °C indicative of the *α-β* transition of quartz. The sample that does not contain cristobalite (*Wall 1)* only shows the *α-β* transition of quartz (also at ~576 °C). Sample *Wall* 4 has a high background value in the XRD spectrum relative to the background of the protolith. *Wall 4* additionally exhibits minor bulk chemical differences from the protolith (Table 1).

2.7 The protolith on experimental thermal treatment

Subjected to 2 linear heating and cooling cycles to and from 1400 °C at 25 °C.min^{-1}, the protolith undergoes mass loss events on the first heating cycle. Between ~400 and ~1000 °C ~2 % (in Fig. 4 relative mass is displayed as a fraction) of the initial sample mass is lost, and the peak mass loss rate occurs at ~580 °C. There is no detectable mass change on subsequent heating and cooling cycles (Fig. 4). These data are broadly consistent with the loss-on-ignition value for the protolith of 2.84 wt% (to 1300 °C) and the lower value for vitrified sample *Wall 4* of 0.51 wt% (to 1400 °C), measured during sample preparation for XRF analysis (Table 1). The mass-loss behaviour is exceptionally repeatable to within ~0.4 % variation between sample runs.

The α-β transition of quartz is reversible (Fig. 5) and is measured to occur at 575-577 °C for the heating rate and conditions tested over both first and second heating cycles for all samples (n=38; Supplementary Fig. 1). The peak height of the endotherm associated with the α-β transition in quartz is lower with respect to a linear baseline on the second heating cycle when the first heating cycle exceeded ~1000-1050 °C.

At ~1020 °C, an exothermic heat-flow peak is consistently produced (Fig. 5). This exotherm is not reversible, such that if 1020 °C is exceeded on the first heating cycle, this event will not appear on the second heating cycle. However, if the first heating cycle peak-temperature is <1020 °C then this exotherm will appear on the second heating cycle above 1020 °C irrespective of any isothermal dwell at peak temperature (Fig. 5C & 5D).

Where the heating program did not exceed ~1000-1050 °C the mineralogy of the experimental samples is almost identical to that of the protolith. However, if the sample is taken above this temperature range, then the peaks in the XRD pattern of the experimental samples differ from those of the protolith. Namely, the quartz peaks at 20.8 and 26.6° 2θ are less intense, the complex feldspar peak at ~28° 2θ is diminished or absent and the primary cristobalite peak appears at 21.8° 2θ (Fig. 6). The absolute experimental peak temperatures after which feldspar is no longer detectable and at which cristobalite appears are dependent on the isothermal dwell time at peak temperature. For example, when no isothermal dwell is applied (0 hours; Fig. 6A), feldspar is detectable in the patterns up to peak temperatures of ~1200 °C and cristobalite is not detectable until peak temperatures of ~1300 °C. However, if an isothermal dwell is applied at the peak temperature before cooling and subsequent measurement (10 or 20 hours; Fig. 6B & 6C), then feldspar is seen to be removed by ~1000 °C and cristobalite is already detectable at ~1200 °C. This time-dependence of reactions involving the removal or appearance of phases in our analysis is further quantified by the integration procedure described in Section 2 and illustrated in Fig. 7. The feldspar peak is too complex for direct integration (it consists of a peak triplet), but the clean peaks of quartz and cristobalite yield peak areas that can be taken relative to those in the protolith (Fig. 2). Such analysis is consistent with all other findings such that changes in mineralogy occur at peak temperatures >1000-1050 °C and are time- and temperature-dependent.

The low-angle background intensities in the XRD patterns are qualitatively higher relative to the background in the protolith for treated samples that exceeded ~1200 °C.

3. Model constraints of vitrification feasibility

3.1 The effect of grain-size on vitrification feasibility

Rocks exposed to externally applied temperatures will develop an internal thermal gradient and take a finite time to reach thermal equilibrium. The time required for thermal equilibrium is strongly dependent on particle size. When applying our results performed on fine-grained powders of sandstone to the boulders found at Wincobank site, we can consider this effect using a 1D numerical solution to the heat equation for the evolution of a temperature profile inside a material as a function of particle size and time.

In spherical coordinates, the evolution of temperature T as a function of radial spatial position r and time t without dissipation is given by recasting Fick's second law

$$\frac{\partial T}{\partial t} = \frac{1}{r^2}\frac{\partial}{\partial r}\left(r^2 D \frac{\partial T}{\partial r}\right)$$

where T is the absolute temperature and D is the thermal diffusivity of the material. The temperature dependence of the thermal diffusivity in quartz or in sandstone is poorly constrained and so, for illustrative purposes, we choose a constant diffusivity for the conditions constrained in this work (T=1250°C) such that D=10^{-7} $m^2.s^{-1}$. This agrees well with an extrapolation of the experimental constraint on the thermal diffusivity of quartz to temperatures in this region of interest (Kanamori, et al., 1968) and with estimates for sandstones from a similar location in the U.K. (Wilson and Luheshi, 1987). We take initial and boundary conditions where T_i is the instantaneously applied external temperature and T_0 is the initial temperature internal to the particle of radius R so we have

$$\begin{cases} T = T_0, \text{ for } r < R, \text{ at } t = 0 \\ \dfrac{\partial T}{\partial r} = 0, \text{ for } t > 0, \text{ at } r = 0 \\ T = T_i, \text{ for } t > 0, \text{ at } r = R \end{cases}$$

We solve Eq. 1 numerically using a finite difference method for which the absolute spatial step size is 5 % of the particle radius and the time-step is derived from the CFL condition (see Supplementary Information for details). This yields a dimensional result for the temporal evolution of the distribution of temperature in a particle of a given size. Furthermore, by taking a sandstone matrix density ρ equivalent to quartz of 2650 $kg.m^{-3}$, a thermal conductivity k of the matrix at elevated temperature of 2.0 $W.m.K^{-1}$ and heat capacity C_p of 2000 $J.kg^{-1}.K^{-1}$

(Vosteen and Schellschmidt, 2003), we can employ a scaling of the thermal diffusivity associated with porosity ϕ (Connor, et al., 1997)

$$D = \frac{k}{\rho C_p (1-\phi) + \rho^g C_p^g \phi} \quad (0.1)$$

where the superscript g denotes the values for the pore fluid rather than the matrix. We take air as the pore fluid and ϕ=*0-0.3* typical for sandstones at varying degrees of diagenesis (e.g. Hallsworth & Chisholm, 2000). This equips us with a tool for assessing the thermal gradient in porous sandstone particles. By setting a threshold at which we consider the particle in thermal equilibrium as when the temperature at r=0 reaches 1 % of T_i, we can show that the time required for equilibrium scales with the particle size and is dependent on the porosity (Fig. 8). Further solutions varying the temperature outside the particle between 900 and 1300 °C produce very similar results.

4. Discussion

4.1 Determination of temperatures and timescales required for vitrification

4.1.1 Evidence from mass loss

In our experimental suite, the most significant mass loss event occurs at 500-700 °C. None of the wall samples measured showed any mass loss event within the analytical error. This agrees with the loss-on-ignition value of 0.51 wt% for the vitrified sample *Wall 4*, which is significantly less than that for the protolith (2.84 wt%; Table 1). Therefore, the wall samples all likely reached temperatures at least greater than the temperature at which we record the peak mass loss rate ~580 °C (Fig. 4). This further suggests that there has been negligible hydration of the wall samples since the Iron Age. The bulk composition of the most vitrified sample from the Wincobank site wall (*Wall 4*) and that of the protolith are similar and so we do not invoke mass loss as a mechanism for significant volatilisation of any particular chemical constituent (Table 1). The mass loss is most likely controlled by the decomposition of the kaolinite and muscovite components, which are not present after the initial heating cycle or in the vitrified samples.

4.1.2 Evidence from cristobalite

Cristobalite is present in samples extracted directly from the vitrified portions of the Wincobank site wall (Fig. 3). We experimentally verify that in our SiO_2-rich, quartz dominated system, cristobalite can readily form at temperatures >1200 °C in times <10 hours or at temperatures >1000 °C in times >10 hours. This is seen as the 21.8° 2θ peak in the XRD patterns of our post-experimental samples (Fig. 6) and in the DSC data for the second heating (Fig. 5), evidenced by the α-β cristobalite transition at ~170-270 °C (e.g. Damby, et al., 2014). The consistent dependence of cristobalite content on temperature and on time in our experimental samples (Fig. 7) shows that the kinetics in this crystallisation process are as critical as the absolute peak temperature up to the first 10 hours. This implies that equilibrium conditions are met at times greater than 10 hours.

Cristobalite was also detected in samples from the fort wall of Sainte Suzanne in France by Smith and Vernioles (1997) using Raman spectroscopy. For these authors, the presence of cristobalite was indicative of vitrification temperatures up to or in excess of the thermodynamically stable formation temperature for cristobalite of 1470 °C. While they admit that cristobalite has been shown to exist in a metastable form below this stability field, they conclude that these high temperatures have potential implications for the thermal technology available to Iron Age fort-builders or attackers.

We propose that the exothermic event in our heat flow data at ~1050 °C (Fig. 5) is consistent with the transition between β-quartz and β-cristobalite, which is known to be possible in

systems that are not able to form the intermediate *β*-tridymite (Heaney, 1994). In such systems, *β*-cristobalite can readily form at metastable temperatures from *β*-quartz and this explains the consistent evidence for cristobalite in our experimental samples. On these grounds we do not hold with Smith and Vernioles (1997) that the mere presence of cristobalite can be correlated with temperatures of formation at mineral stability without more sophisticated consideration and dispute their claim that vitrification necessarily reached 1470 °C. This assertion is further supported by previous work showing metastable formation of cristobalite in experimental (e.g. Chao and Lu, 2002) and natural (e.g. Horwell, et al., 2013) systems. Further, Stevens et al. (1997) show that the (pure) quartz to cristobalite transformation below 1400 °C is promoted by a mineraliser, suggesting the breakdown of feldspar (section 4.1.3) and/or phyllosilicates (section 4.1.1) may facilitate cristobalite formation in our samples; however, this is not further investigated.

Using this experimental constraint, we can approach an interpretation of the presence of cristobalite in the samples from the vitrified wall at the Wincobank site. Three of the four wall samples analysed here contain cristobalite. Therefore, we propose that these 3 samples reached approximate temperatures of ≥1050 °C. The XRD patterns show that, relative to the protolith, cristobalite does indeed incrementally increase as the experimental temperature exceeds 1100 °C (Fig. 7). Furthermore, the inclusion of an isothermal dwell (10 or 20 hours) results in an increase in the relative abundance of cristobalite stabilised and preserved on cooling.

Using the cristobalite peak in the XRD patterns for the Wincobank wall samples relative to the same position in the protolith pattern and comparing this relative measure of abundance with the experimental findings, we suggest that the 3 cristobalite-containing Wincobank wall samples (*Wall 2, Wall 3 and Wall 4*) are most consistent with a window between ~1100 °C (*Wall 2*) to temperatures higher than we used in our experiments (e.g. ~1450 °C; *Wall 4*) for 0 hours or between 1050 °C (*Wall 2*) to 1225 °C (*Wall 4*) for >10 hours. We suggest that the remaining wall sample, which does not contain cristobalite (*Wall 1*), did not reach this critical temperature (1050 °C) at any time. In turn, this suggests that the peak temperature reached in the wall is spatially variable.

4.1.3 Evidence from feldspar

Feldspar is the second most abundant phase in the protolith and is only present in sample *Wall 1* from the Wincobank site wall. Using a similar method of relative abundance quantification to that used for cristobalite or quartz (Fig. 7) has not been possible because feldspar exhibits a complex peak in XRD patterns and no obvious thermal transition manifest in heat flow data. However, qualitatively, we can see that the peak associated with feldspar in the XRD patterns from our post-experimental samples is no longer discernible if the protolith was heated to 1300 °C for 0 hours or ~1100 °C for >10 hours. The peak height is broadly a negative function of temperature, suggesting qualitatively that the feldspar is being progressively removed during heating. This would additionally suggest that the sample *Wall 1* did not exceed the window above which feldspar is depleted, but samples *Wall 2, Wall 3* and *Wall 4* did indeed exceed

1100-1300 °C. This is highly consistent with the constraint from cristobalite, as discussed above.

4.1.4 Evidence from quartz

The relative abundance of quartz, derived by comparing the integrated quartz peaks in the XRD patterns of the post-experimental samples with that for the protolith, yields a depletion of quartz as temperature is increased. As with cristobalite, this is only apparent in the data for samples that experienced >1100 °C. Similarly, this process appears to be time dependent such that after 0 hours at peak temperature the relative abundance of quartz remaining in the sample is greater than after >10 hours at peak temperature (Fig. 7). The data acquired by integrating the endothermic peak in the heat flow data produced over the α-β transition in quartz on the second heating cycle of the protolith and taking this relative to the same transition seen on the first heating cycle, yields remarkably good agreement with the XRD-derived values (Fig. 7A).

Using the same method of comparing the Wincobank wall sample data relative to the protolith with that from the experimental suite yields comparable relative quartz abundances (Fig. 7). By this analysis we find that *Wall 2* is consistent with a minimum firing temperature of 1200 °C for >10 hours, *Wall 3* is consistent with ~1250 °C for >10 hours and *Wall 4* is outside of the measured range. *Wall 1* gives an apparent minimum 10 hour firing temperature of 1050-1100 °C, however, due to the absence of cristobalite in this sample, we suggest that it did not, in fact, reach 1020 °C for any time (section 4.1.3) and was fired to a lower temperature.

4.1.5 Evidence from glass

An endothermic DSC peak attributable to a glass transition appears on second heating in the heat flow data for samples for which feldspar had been completely depleted and one might expect a melt phase to have formed. For samples heated to 1250 °C on the first heating cycle, the extrapolated onset of this glass transition occurs at ~1010 °C and 980 °C for a 0 and 10 hour isotherm, respectively (Fig. 5). The glass transition estimated for such a composition (using the model of Giordano et al., 2008) for a heating rate of 25 °C.min^{-1} is ~984 and ~1004 °C if we use the composition of *Wall 4* or the protolith (Table 1) as inputs respectively (see Supplementary Information). Although this is an extrapolation of the viscosity model it is nevertheless consistent with the onset of the endothermic signal observed in the vitrified samples in the range of 950-1000 °C. If this glass transition assignment is correct then the physical deformation and flow of these glassy layers would be restricted to temperatures above this value. Glass transition temperatures for very high silica compositions of the kind used here are notoriously difficult to detect.

A qualitative increase in the baseline of the XRD pattern between ~10-40 deg 2theta on the XRD patterns (figure?), interpreted as evidence for an amorphous phase due to the lack of long-range atomic order, suggests the production of a glass phase from a supercooled melt that is quenched in the samples. An increasing melt content as samples approach the liquidus from the

403 solidus is expected and, coupled with the conversion of quartz to cristobalite, provide a clear
404 conceptual model for the evolution of the protolith as it undergoes thermal alteration.

405

406 4.2 The temperature-time window for vitrification of the Wincobank hill fort wall

407 Constraints of vitrification temperatures have, to date, been for broadly granitic composition
408 building materials used in many vitrified hill fort walls, for which a dry solidus and liquidus
409 temperature ranges between 925 °C and 1000-1250 °C, respectively (e.g. Youngblood et al.,
410 1987; Brothwell, 1984; Friend et al., 2008). These have been used as bracketing values such
411 that, in order to produce any melt capable of vitrification on cooling, the rock has to be heated
412 above the solidus, and to preserve primary crystal phases observed, the rock cannot exceed the
413 liquidus. However, this is complicated by the experimental evidence for quench crystallisation
414 (Hearne, 2015; Friend et al., 2008). Additional complications involve the effect of redox state
415 (Youngblood et al., 1978) and hydrous minerals on the solidus and liquidus; for example Friend
416 et al. (2007) invoke biotite as a candidate for a relatively low-temperature melting scenario
417 (~850 °C) in the rocks from a psammite protolith. One anomalous study proposes exceptionally
418 high temperatures of vitrification based on the preservation of cristobalite (Smith and Vernioles,
419 1997) which we discuss above (section 4.1.2). Other than this exception, the temperature ranges
420 proposed in the literature to date are reasonably consistent regardless of lithology and have been
421 demonstrated to be feasible in large-scale (Ralston, 1987; Childe & Thorneycroft, 1932) and
422 sample-scale experimentation (Hearne, 2015; Friend et al., 2008).

423 The kinetics of melting have been routinely overlooked. Many temperature estimates are based
424 on thermodynamic models that were usually compiled from equilibrium experiments. Kinetic
425 processes are alluded to by Youngblood et al. (1978), who states that there is a
426 "time…necessary to melt the rocks." Kinetics are explicitly explored by Hearne (2015) who
427 investigates the difference between relatively long and short experiments over the range 850-
428 1325 °C. We find that for our samples the kinetic effect is only relevant at heating times <10
429 hours such that equilibrium is approached at these times.

430 In the above sections we have shown that the measured abundances of quartz and cristobalite
431 can be consistent with a range of temperatures for different times of high temperature treatment.
432 If we consider the upper temperature limits – which are if those temperatures were achieved
433 only for very short times - to be higher than were generally attainable with Iron Age technology,
434 then we could argue that the wall was heated to a lower temperature for a comparatively longer
435 time. Therefore, in synthesis, we find it most useful to provide the lowermost limits from our
436 experimental constraints that would consistently explain all data. This approach yields minima
437 in the range <1020 °C (*Wall 1*) and 1250 °C (*Wall 3*; >10 hours). The differences between the
438 estimates attained for each wall sample is a testament to the differential heating often observed
439 in vitrified fort walls (e.g. Hearne, 2015; Friend et al., 2007). We consider the dominant factor
440 affecting this differential vitrification would be heat transfer through the wall, which is highly
441 block-size dependent (Fig. 7). Heat transfer would be facilitated if a timber-frame were
442 providing heat internal to the wall, which is often thought to have been the case at vitrified fort
443 sites (e.g. Ralston, 1986). If a vitrified fort were to show a thoroughly vitrified wall, then it

444 would follow that the firing timescale were at least equivalent to the heat transfer timescale.
445 This is certainly the case on the block-scale where it is often the periphery of blocks which are
446 vitrified while the inside is not (Fig. 1) or where the small grains interstitial to the larger blocks
447 in the wall are thoroughly vitrified while the large blocks are intact.

448

449

5. Conclusions

Here we constrain the temperature and timescales of vitrification at the Wincobank site using the sandstone protolith from which the fort walls are constructed as an experimental starting material. We use XRD and thermal analysis (DSC and TG) to constrain the mineralogical changes that occur on heating of the protolith to 600-1400 °C. We compare these data to vitrified wall samples found in-situ at the same Wincobank site, finding that cristobalite is present in vitrified samples and not in the protolith and feldspar has been removed. We find self-consistency in our temperature and timescale estimates derived from the evolution of cristobalite, quartz, feldspar, glass and sample mass, providing minimum estimates of <1020-1250 °C for >10 hours. Finally, we highlight that vitrification at this site was highly variable and explore the reasons for variable thermal treatment using a 1D numerical solution to the heat equation.

Acknowledgments

We thank Michael Heap for a thorough and constructive review, Donjá Aβbichler and Nick Marsh who measured the bulk compositions by XRF and to Roger Doonan for providing samples from the University of Sheffield. We acknowledge funding provided by the European Union's seventh program for research, technological development and demonstration under grant agreement VUELCO (282759) and the European Research Council for funding the Advanced Investigator Grant EVOKES (247076).

References Cited

Beswick, P., 1985. Wincobank hillfort drainage scheme: Archaeological report. Transactions of the Hunter Archaeological Society 13, 29-33.

Beswick, P., 1987. Wincobank hillfort: Radiocarbon dates. Prehistory Research Section Bulletin of the Yorkshire Archaeological Society 24, 6.

Bowden, M., McOmish. D. 1987. The required barrier. Scottish Archaeological Review 4, 76-84.

Brothwell, D., Bishop, A., Woolley, A., 1974. Vitrified forts in Scotland: a problem in interpretation and primitive technology. Journal of Archaeological Science 1, 101-107.

Chao, C.-H., Lu, H.-Y., 2002. β-Cristobalite stabilization in (Na2O+ Al2O3)-added silica. Metallurgical and Materials Transactions A 33, 2703-2711.

Childe, V.G., Thorneycroft, W., 1938. The experimental production of the phenomena distinctive of vitrified forts.

Connor, C., Lichtner, P., Conway, F., Hill, B., Ovsyannikov, A., Federchenko, I., Doubik, Y., Shapar, V., Taran, Y.A., 1997. Cooling of an igneous dike 20 yr after intrusion. Geology 25, 711-714.

Cotton, M., 1954. British camps with timber-laced ramparts. Archaeological Journal 111, 26-105.

Damby, D.E., Llewellin, E.W., Horwell, C.J., Williamson, B.J., Najorka, J., Cressey, G., Carpenter, M., 2014. The α-β phase transition in volcanic cristobalite. Journal of applied crystallography 47, 1205-1215.

Friend, C., Dye, J., Fowler, M., 2007. New field and geochemical evidence from vitrified forts in South Morar and Moidart, NW Scotland: further insight into melting and the process of vitrification. Journal of Archaeological Science 34, 1685-1701.

Friend, C., Charnley, N., Clyne, H., Dye, J., 2008. Experimentally produced glass compared with that occurring at The Torr, NW Scotland, UK: vitrification through biotite melting. Journal of Archaeological Science 35, 3130-3143.

Hallsworth, C., Chisholm, J., 2000. Stratigraphic evolution of provenance characteristics in Westphalian sandstones of the Yorkshire Coalfield. Proceedings of the Yorkshire Geological and Polytechnic Society, Geological Society of London, pp. 43-72.

Heaney, P.J., 1994. Structure and chemistry of the low-pressure silica polymorphs. Reviews in Mineralogy and Geochemistry 29, 1-40.

Hearne, R.L., 2015. Vitrification at Iron Age Hillforts in Northern England: A Multidisciplinary Investigation. Prehistoric Yorkshire 52, 111-124.

Horwell, C.J., Williamson, B.J., Llewellin, E.W., Damby, D.E., Le Blond, J.S., 2013. The nature and formation of cristobalite at the Soufrière Hills volcano, Montserrat: implications for the petrology and stability of silicic lava domes. Bull Volcanol 75, 1-19.

Kanamori, H., Fujii, N., Mizutani, H., 1968. Thermal diffusivity measurement of rock-forming minerals from 300° to 1100° K. Journal of Geophysical Research 73, 595-605.

Kresten, P., 2004. The Vitrified forts of Europe: saga, archaeology and geology. Applied Mineralogy: Developments in Science and Technology, Sao Paolo, 355-357.

MacKie, E., 1969. Timber-laced and vitrified walls in Iron Age forts: causes of vitrification. Glasgow Archaeological Journal, 69-71.

MacKie, E.W., 1976. The vitrified forts of Scotland, Hillforts, Later Prehistoric Earthworks in Britain and Ireland. Academic Press, London, 205-235.

Nisbet, H.C., 1974. A geological approach to vitrified forts. Sci. Archaeol 12, 3-12.

Ralston, I., 1986. The Yorkshire Television vitrified wall experiment at East Tullos, City of Aberdeen District. Proceedings of the Society of Antiquaries of Scotland, National Museum of Antiquities of Scotland, pp. 17-40.

Small, A., Cottam, M., 1972. Craig Phaidrig. University of Dundee, Department of Geography, Occasional papers 1.

Smith, D.C., Vernioles, J.D., 1997. The Temperature of Fusion of a Celtic Vitrified Fort: a Feasibility Study of the Application of the Raman Microprobe to the Non-Destructive Characterization of Unprepared Archaeological Objects. Journal of Raman spectroscopy 28, 195-197.

Stevens, S., Hand, R., Sharp, J., 1997. Temperature dependence of the cristobalite α-β inversion. Journal of thermal analysis 49, 1409-1415.

Vosteen, H.-D., Schellschmidt, R., 2003. Influence of temperature on thermal conductivity, thermal capacity and thermal diffusivity for different types of rock. Physics and Chemistry of the Earth, Parts A/B/C 28, 499-509.

Wilson, N., Luheshi, M., 1987. Thermal aspects of the East Midlands aquifer system. Geological Society, London, Special Publications 34, 157-169.

Youngblood, E., Fredriksson, B., Kraut, F., Fredriksson, K., 1978. Celtic vitrified forts: implications of a chemical-petrological study of glasses and source rocks. Journal of Archaeological Science 5, 99-121.

Table 1 Bulk chemical composition (wt.%)

Oxide	Protolith	Wall 4
SiO_2	83.05	83.53
Al_2O_3	7.82	9.79
Fe_2O_3	2.38	2.01
MnO	0.04	0.02
MgO	0.40	0.63
CaO	0.06	0.14
Na_2O	0.92	1.12
K_2O	1.28	1.57
TiO_2	0.92	0.67
P_2O_5	0.07	0.08
LOI	2.84	0.51
Total	99.78	100.08

measured by powder X-ray fluorescence

564

565

Figure 1 (black and white)

A photograph of a vitrified sample from the wall at the Wincobank site, Yorkshire, U.K. (reproduced with permission from Hearne, 2015). The scale bar at the base of the sample is divided into centimetres.

571 **Figure 2 (black & white)**

572 Detail of the diffraction pattern from the unaltered wall material (the experimental protolith)
573 showing that it is dominantly composed of quartz (Qz) and feldspar (Fsp) with muscovite
574 (Musc.) and kaolinite (Kaol.) components (*see text*) diffracting at low angles 2θ.

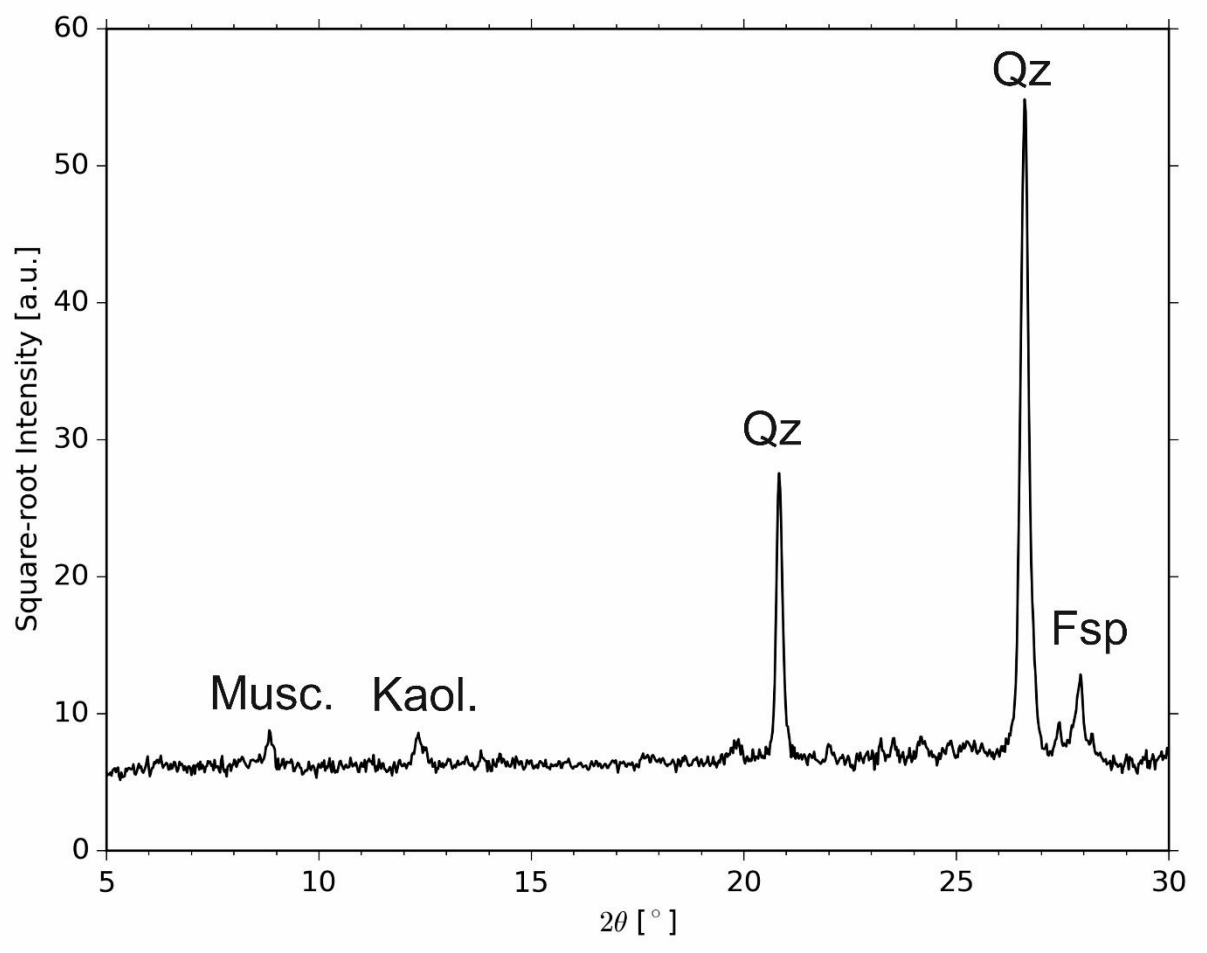

575

576

Figure 3 (black and white)

Details of the X-ray diffraction patterns for the 4 variably altered wall samples analysed here showing that they are composed of variable amounts of quartz (Qz) with trace amounts of feldspar (Fsp) in sample *Wall 1* and varying amounts of cristobalite (Cr) in samples *Wall 2*, *Wall 3* and *Wall 4*. Trace sekaninaite (Sk) appears to be present in samples *Wall 2* and *Wall 3*.

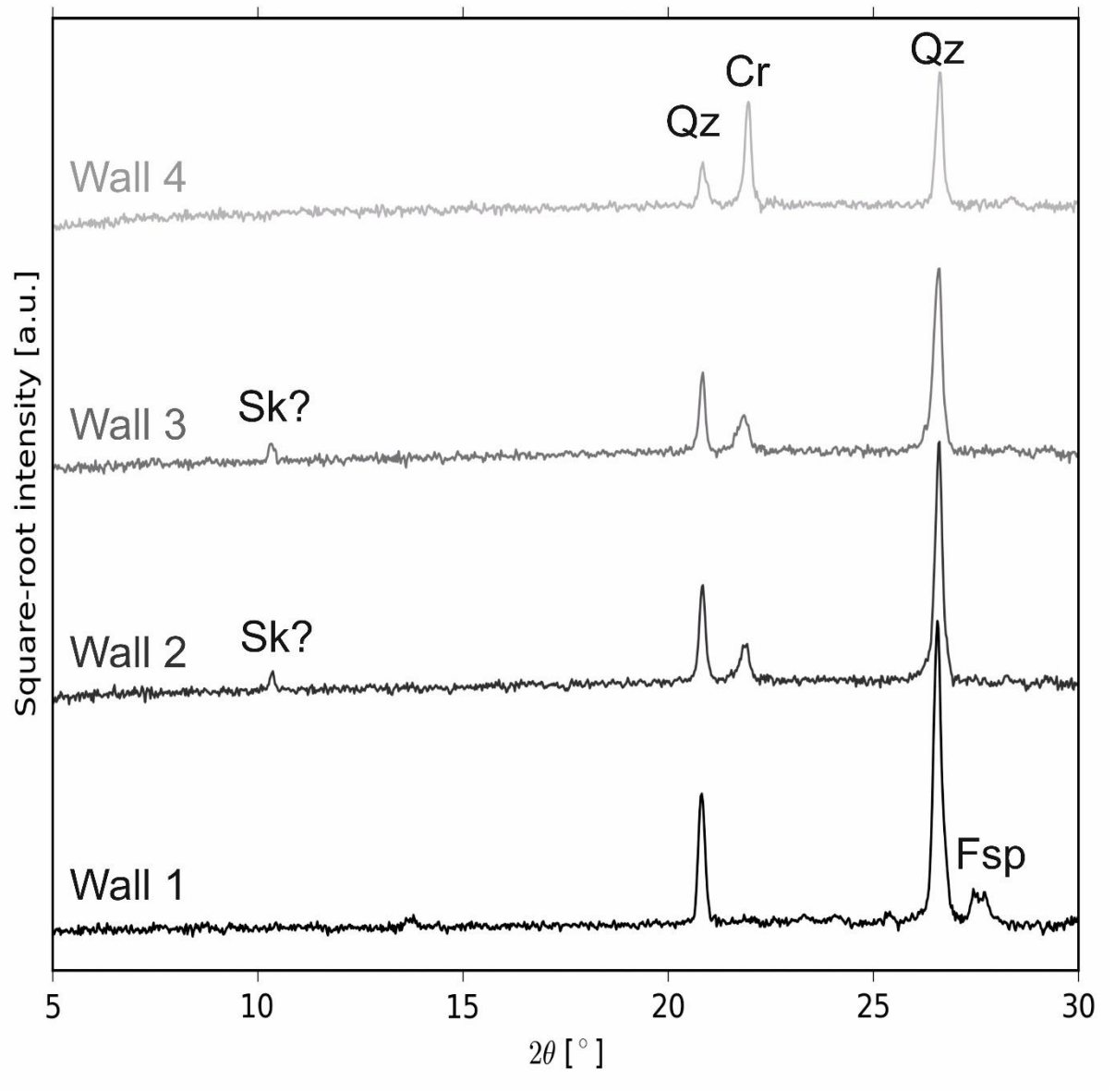

Figure 4 (black and white)

(A) Changes in the experimental protolith sample mass relative to the initial mass of the protolith during 2 heating cycles at 25 °C.min^{-1} to 1300 °C and no isothermal time at high temperature. The curves are a single representative measurement and the deviation among runs (n=12) was <2 %. (B) The peak mass loss rate occurs at ~580 °C and total mass lost ~0.02 %. The second heating and both cooling cycles are thermally stable and produce repeatable mass signals.

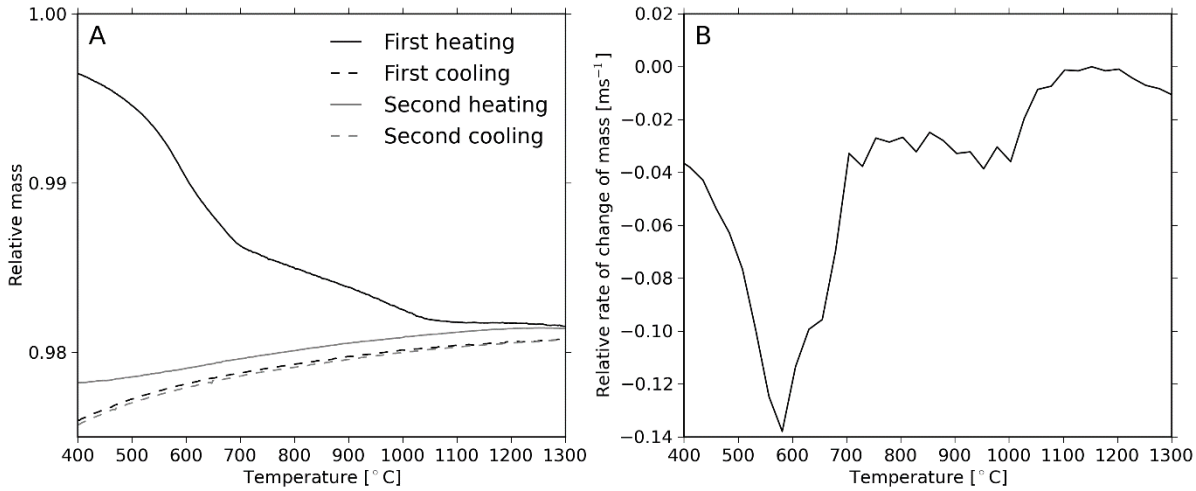

Figure 5 (colour)

The heat flow response on a 2-cycle heating program at 25 °C.min^{-1} with (A) no isothermal time at high temperature or (B) with a 10 hour isothermal time at peak temperature. *Inset*: the emergence of a peak at 218 °C for the sample heated to 1300 °C attributed to the α-β transition of cristobalite (peak labelled "1"). $T_{g,onset}$ refers to the onset of the glass transition. (C) The heat flow response on the first heating cycle to high temperature for which each curve terminates at the respective peak temperature. (D) The thermal response on a second heating cycle where the colours indicate the peak temperature reached on the first heating cycle in panel C.

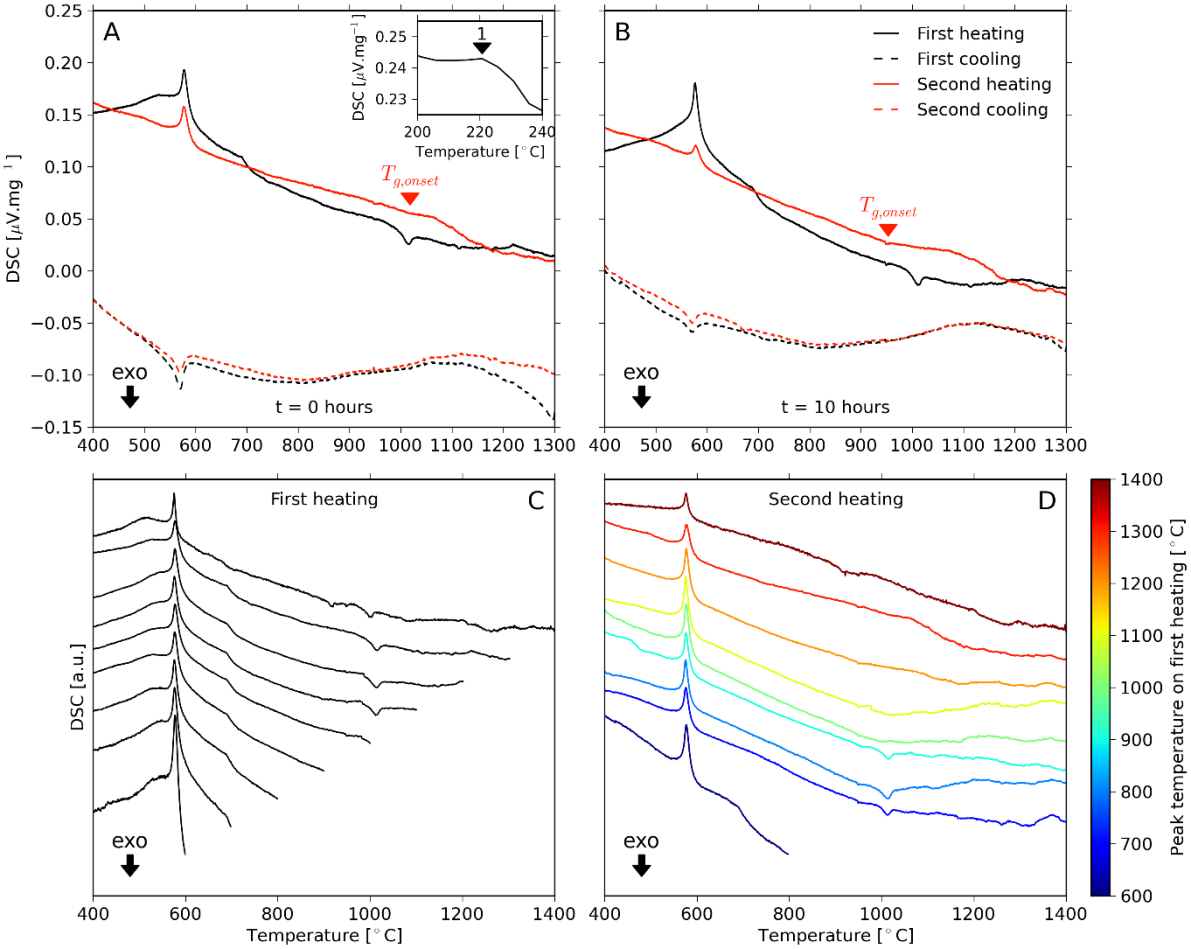

606 **Figure 6 (black and white)**

607 Stacked X-ray diffraction patterns for thermally treated protolith samples (Fig. 1 for pristine
608 XRD pattern) produced after heating at 25 °C.min^{-1} to a peak temperature and held for (A) 0
609 hours, (B) 10 hours and (C) 20 hours before cooling to ambient conditions.

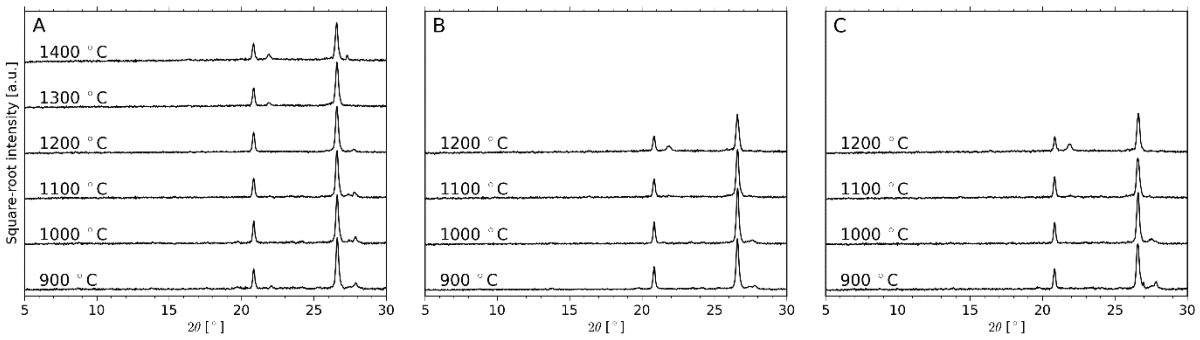

610

611

Figure 7 (black and white)

The relative abundance of (A) quartz and (B) cristobalite in the experimentally treated samples as a function of peak temperature and normalised to the abundance in the unaltered protolith sample. (A) Quartz data were acquired using both the calorimetric heat flow data and the X-ray diffraction pattern. Using the heat flow data, the endothermic peak at ~576 °C for the second heating cycle was integrated over the range 560-600 °C and normalised to the same integrated peak from the equivalent first heating cycle on the same sample. For the X-ray diffraction data, the baseline-subtracted peak at 26.6° 2θ was integrated and also normalised to the protolith value. (B) The baseline-subtracted peak at 21.2° 2θ in the XRD pattern was integrated and normalised to the value in the protolith pattern. In both cases, a deviation from a value of 1 (dashed lines) indicates changes due to the thermal treatment.

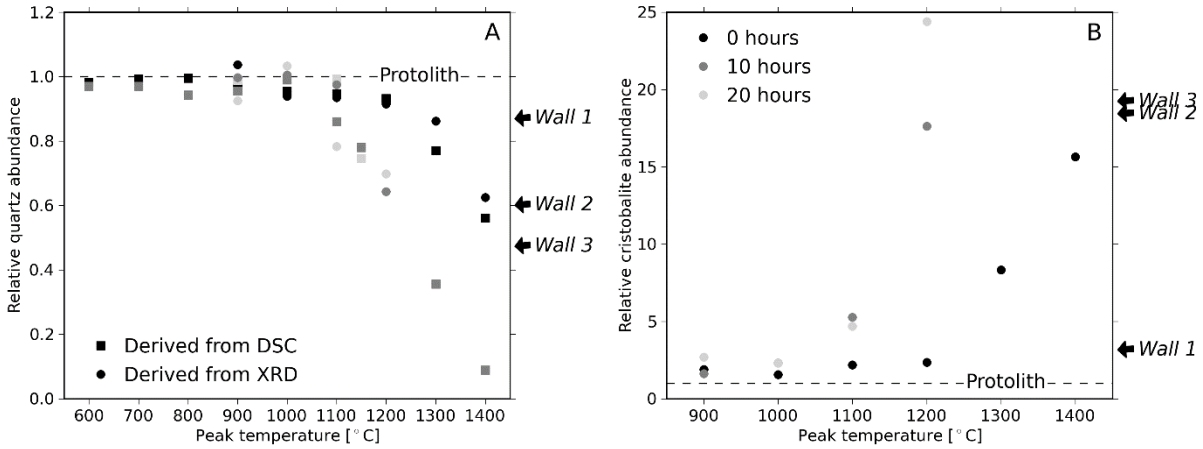

Figure 8 (black and white)

The results of the numerical solution to the 1D heat equation cast in spherical coordinates (Eq. 1) with the effect of sample gas volume fraction considered up to 0.3 (Eq. 3) and with a threshold for thermal equilibrium defined as when the particle centre is within 1% of the applied external temperature. These results show that the size of the block in the wall strongly controls how thoroughly the temperature, and thus the vitrification potential, is distributed internally.

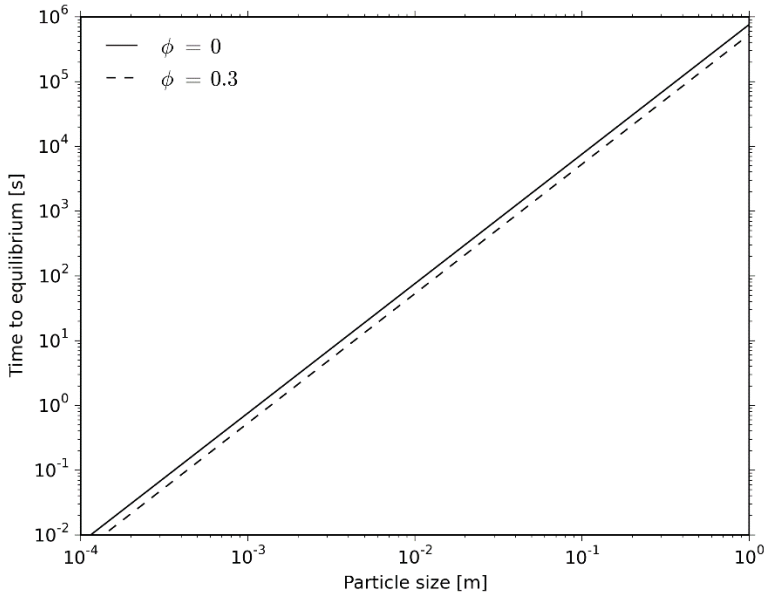

Supplementary information

Fabian B. Wadsworth[1], David E. Damby[1], Rebecca L. Hearne[2,3], Jennifer S. Le Blond[4,5], Jérémie Vasseur[1], Jens Najorka[5], Kai-Uwe Hess[1], Donald B. Dingwell[1]

Supplementary figure 1

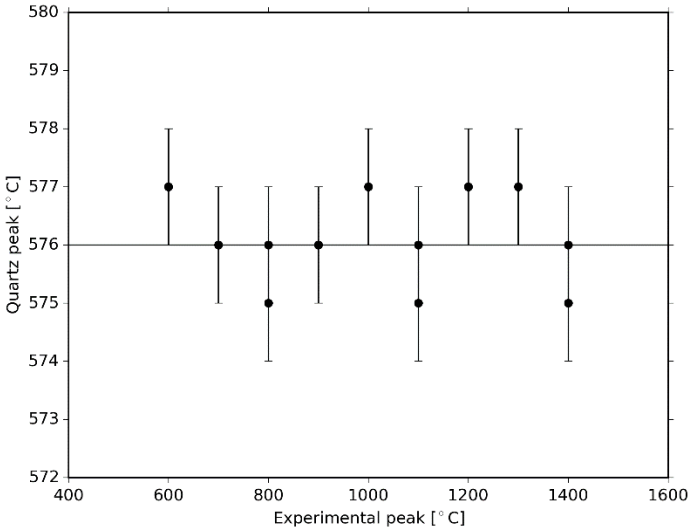

The thermal position of the peak in the α to β transition in quartz as a function of the experimental conditions used. Note that the position is within 1 °C of the analytical error on temperature determination and is therefore considered to be stable and independent of the thermal treatment conditions. And note that the absolute position is heating rate dependent, but what is critical is that for the conditions used, it is repeatable and not affected by heat treatment.

646 **Courant-Freidrichs-Lewy (CFL) stability condition for the thermal model**

647 For a stable numerical solution to the heat equation (Eq. 1), we must define the spatial and
648 temporal step sizes in our finite difference scheme. As stated in the model description, we use
649 a spatial step Δr that is 5 % of the radius R of the particle in question, so that for R=1 m we
650 would take a spatial step of 5 cm. In this example, we can use the CFL stability condition as
651 follows

652 $$\frac{2D\Delta t}{\Delta r^2} \leq \frac{1}{2}$$

653

654 to define the appropriate time step Δt we should use. In the example of a 1 m radius particle, and the
655 diffusivity D discussed in the model description, we would therefore take Δt=5.26 hours in order to
656 ensure stability.

657

658

659 **Glass transition estimation**

660 Using the viscosity model of Giordano et al. (2008) we can input the bulk composition of the
661 protolith or *Wall 4* (Table 1) and predict the temperature dependence of viscosity for? a melt of
662 that composition. This is possible as the model outputs *A*, *B* and *C* parameters used in a Vogel-
663 Fulcher-Tammann equation. Coupling this with a model for the prediction of the viscosity of a
664 melt at the glass transition T_g as a function of cooling rate q permits us to arrange for the thermal
665 position of T_g as a function of cooling rate:

666

667 $$T_g = C + \frac{B}{k - \log_{10}|q| - A}$$

668

669 where k is the so-called melt shift factor. Here we use an accepted value of $k = 10$ and parameters
670 *A*, *B* and *C* from the Giordano et al. (2008) model (Supplementary Table) to find T_g at our
671 experimental cooling rates of 25 $K.min^{-1}$.

672

673 **Supplementary Table**

	Wall 4	Protolith
A	-4.55	-4.55
B	12655.1	13052
C	350.1	341.7

674

675

676 **Supplementary figure 2**

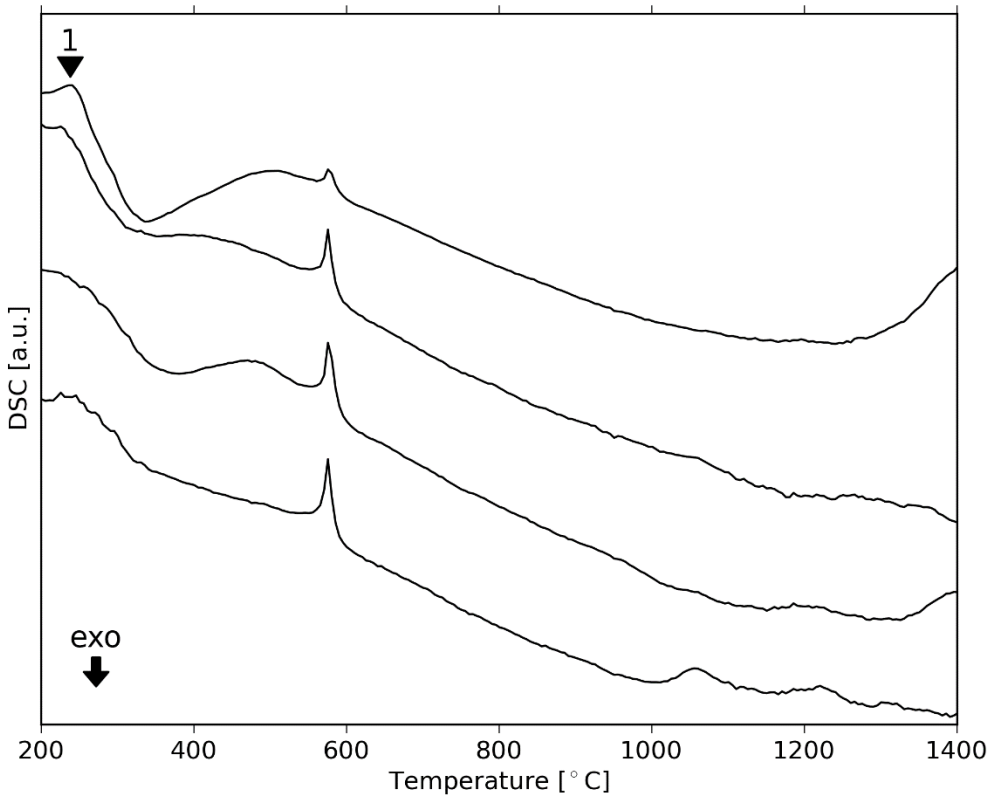

677

678 The DSC signal associated with heating the vitrified samples at 25 K.min^{-1} to 1400 °C. From
679 bottom to top the curves are *Wall 1*, *Wall 2*, *Wall 3* and *Wall 4*. In sample *Wall 4* an arrow
680 labelled "1" refers to the α-β transition of cristobalite, the peak for which occurs at 238.2 °C.

681

682